Real-time monitoring of respiration rhythm and pulse rate during sleep

メタデータ	言語: eng 出版者: 公開日: 2017-10-03 キーワード (Ja): キーワード (En): 作成者: メールアドレス: 所属:
URL	http://hdl.handle.net/2297/6690

Real-Time Monitoring of Respiration Rhythm and Pulse Rate During Sleep

Xin Zhu*, *Student Member, IEEE*, Wenxi Chen*, *Member, IEEE*, Tetsu Nemoto, Yumi Kanemitsu, Kei-ichiro Kitamura, Ken-ichi Yamakoshi, *Member, IEEE*, and Daming Wei, *Member, IEEE*

***Abstract*—A noninvasive and unconstrained real-time method to detect the respiration rhythm and pulse rate during sleep is presented. By employing the *à trous* algorithm of the wavelet transformation (WT), the respiration rhythm and pulse rate can be monitored in real-time from a pressure signal acquired with a pressure sensor placed under a pillow. The waveform for respiration rhythm detection is derived from the 2^6 scale approximation, while that for pulse rate detection is synthesized by combining the 2^4 and 2^5 scale details. To minimize the latency in data processing and realize the highest real-time performance, the respiration rhythm and pulse rate are estimated by using waveforms directly derived from the WT approximation and detail components without the reconstruction procedure. This method is evaluated with data collected from 13 healthy subjects. By comparing with detections from finger photoelectric plethysmograms used for pulse rate detection, the sensitivity and positive predictivity were 99.17% and 98.53%, respectively. Similarly, for respiration rhythm, compared with detections from nasal thermistor signals, results were 95.63% and 95.42%, respectively. This study suggests that the proposed method is promising to be used in a respiration rhythm and pulse rate monitor for real-time monitoring of sleep-related diseases during sleep.**

***Index Terms*—*à trous* algorithm, pulse rate, real-time monitor, respiration rhythm, sleep monitor, wavelet transformation.**

I. Introduction

MANY cardiovascular diseases, such as hypertension, atherosclerosis, stroke, heart failure, cardiac arrhythmias, and sudden death are related to sleep disturbances [1]. Real-time monitoring of respiration rhythm as well as heart rate during sleep plays an important role in the diagnosis and treatment of disorders like sleep apnea, sudden death syndrome [2], and heart diseases [3]–[5]. In the daily life, the monitoring of respiration rhythm and heart rate during sleep may be tools for the prevention and early diagnosis of adult diseases like obesity, arrhythmias, and coronary artery diseases. They are also used in the home healthcare for the monitoring of patients and seniors' healthy status [6]. There are numerous conventional methods for respiration measurement, such as spirometry, nasal thermocouples, body volume changes, inductance pneumography, impedance plethysmography, strain gauge measurements of thoracic circumference, pneumatic respiration transducers, whole-body plethysmography [6], the fiber-optic sensor method [7], photoplethysmography [8], the Doppler radar [9], and electrocardiogram (ECG)-based derived respiration measurements [10]–[12]. However, all these methods may bring discomfort and inconvenience to the subject and physician because the sensor must be placed on the body or the sensor is expensive for practical use and hard to manipulate. Heart rate monitoring based on vital signs, such as the ECG, heart sounds, and finger photoelectric plethysmography (FPP), also requires appropriate sensors to be installed on the subject. Recently, Nakajima *et al.* [13] developed a low-cost pillow-shaped respiratory monitor to meet the noninvasive and unconstrained requirements of respiration measurement. Watanabe *et al.* [14] have devised a new instrument to measure pressure changes within two water-filled vinyl tubes under a pillow. Because the main signal components in the respiration rhythm (about 10–20 min^{-1}) and pulse rate (about 50–80 min^{-1}) are in different frequency bands, Watanabe *et al.* applied a low-pass filter with a pass band of 0.1–0.8 Hz, to obtain the respiration rhythm; and estimated the pulse rate directly from the raw signal using the peak detection method. Uchida *et al.* [15] employed the independent component analysis (ICA) method to separate useful signals from noise by using two channels of pressure signals. Kanemitsu *et al.* [16] used power spectral density (PSD) to estimate respiration rhythm and heart rate from the frequency domain.

The wavelet transformation (WT) has found many applications in the biomedical signal processing field [17]. WT multiresolution analysis can be applied to detect ECG characteristic points [18], to perform data compression [19], to extract the fetal ECG [20], and to delineate ECG [21]. Chen *et al.* [22] have successfully developed a batch method based on Mallat's algorithm [23] to extract waveforms for detecting the respiration rhythm and pulse rate from a pressure signal measured with an under-pillow sensor. However, real-time estimation of the respiration rhythm and pulse rate remained unresolved.

Manuscript received August 3, 2005; revised May 21, 2006. This work was supported in part by the University of Aizu, Kanazawa University, and SRI R&D Ltd. *Asterisks indicates corresponding authors contributed equally to this work.*

*X. Zhu is with the Graduate Department of Information Systems, University of Aizu, Aizu-Wakamatsu, Fukushima 965-8580, Japan (e-mail: zhuxin@u-aizu.ac.jp).

*W. Chen is with the Department of Computer Science and the Graduate Department of Information Systems, University of Aizu, Fukushima 965-8580, Japan (e-mail: wenxi@u-aizu.ac.jp).

T. Nemoto is with the Department of Laboratory Sciences, School of Health science, Faculty of Medicine, Kanazawa University, Ishikawa 920-1192, Japan.

Y. Kanemitsu is with the SRI R&D Ltd., Hyogo 651-0072, Japan.

K.-I. Kitamura is with Department of Forefront Medical Technology, Graduate School of Medical Science, Kanazawa University, Ishikawa 920-1192, Japan.

K.-I. Yamakoshi is with the Department of Human and Mechanical Systems Engineering, Faculty of Engineering, Kanazawa University, Ishikawa 920-1192, Japan.

D. Wei is with the Department of Computer Science and the Graduate Department of Information Systems, University of Aizu, Fukushima 965-8580, Japan.

Digital Object Identifier 10.1109/TBME.2006.884641

0018-9294/$20.00 © 2006 IEEE

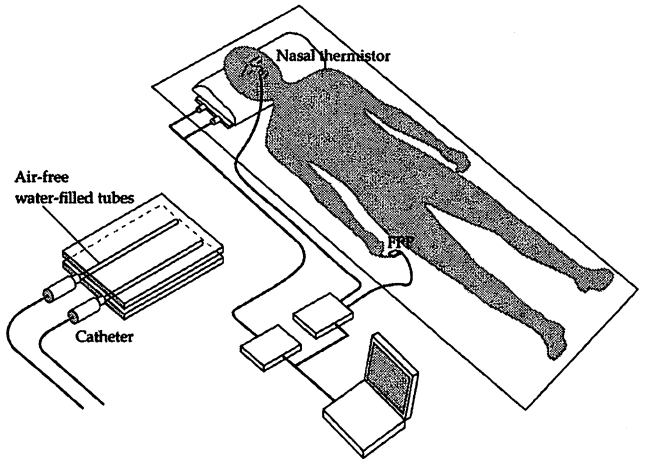


Fig. 1. Schematic of the measurement setup. Two pressure signals are recorded with two under-pillow sensors. FPP and nasal thermistor signals are recorded simultaneously as the reference data.

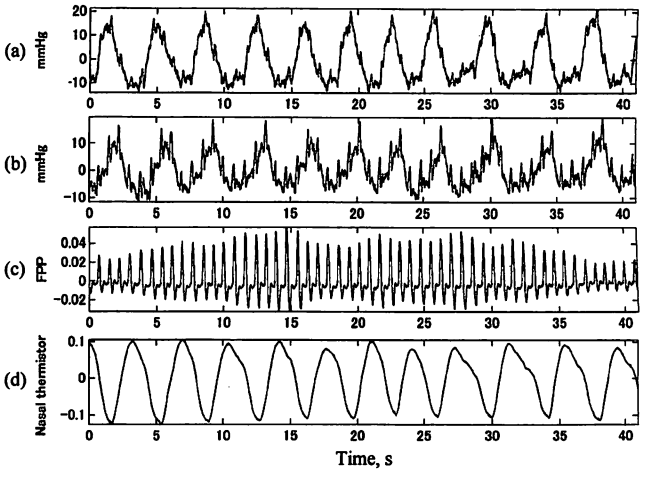


Fig. 2. Four directly measured signals: (a) far-neck occiput pressure, (b) near-neck occiput pressure, (c) FPP, and (d) nasal thermistor signals. Each signal in the figure is 4096 data points in length, or 40.96 s long.

This paper proposes an *à trous* algorithm-based [24] real-time implementation of the respiration rhythm and pulse rate detection from a pressure signal acquired using an air-free water-filled vinyl tube under a pillow during sleep. The measured pressure signal is decomposed into detail and approximation components at multiple scales with the *à trous* algorithm-based method neglecting the re-sampling procedures (down-sampling and up-sampling) and keeping a consistent temporal resolution. Therefore, all of the detail and approximation components are at the same sampling rate. After suppressing random noise with the soft-threshold method [25], respiration- and pulse-related waveforms are obtained from the detail and approximation components in their respective characteristic scales without or with reconstruction procedures. Both respiration rhythm and pulse rate are determined by an algorithm called adaptive characteristic point pursuit by modifying the method described in [28]. The detection accuracy performance was examined with the reference data. Detections without reconstruction procedures were also investigated and compared with those with reconstruction procedures. The results show that the detection accuracies of both methods are very close, but the method without reconstruction procedures requires a shorter processing time and is suitable for real-time applications.

II. Methodology

A. Measurement Setup

A schematic illustration of the measurement system is shown in Fig. 1. Two incompressible vinyl tubes, 30 cm in length and 2 cm in diameter, are filled with air-free water in a preloaded internal pressure of 3 kPa and sandwiched between two acrylite boards, both 3 mm thick, in parallel at a distance of 13 cm from each other. One end of each tube is connected to an arterial catheter. This sensor unit is placed under a pillow during sleep to detect pressure changes beneath the near-neck and far-neck occiput regions. Both static and dynamic components of pressure within tubes are conditioned by bridge amplifiers (KEYENCE Co. Ltd., Japan, Model AP-13, measurement range: 0–1 MPa, repeatability accuracy: below ±0.5% of the full scale) connected to embedded catheters. The static pressure component responds to the weight of a head, and the dynamic component reflects the weight fluctuation of a head due to breathing movements and pulsatile blood flow from the external carotid arteries around the head. After being filtered by an analog filter with a pass band of 0.16–5 Hz, pressure signals are digitized using a 16-bit analog-to-digital (A/D) card in a laptop computer and stored on a digital tape recorder (Sony Corp., PC204A). The pillow is stuffed with numerous fragments of soft comfortable material made of synthetic resins. Signals were collected with this unconstrained noninvasive method during sleep in either a supine or a recumbent position. FPP and nasal thermistor measurements were recorded simultaneously as reference data for evaluating the detection accuracy. The sampling rate was 100 Hz for all four signals.

Fig. 2 shows 4096 samples of typical measured data, or 40.96 s in time. The upper two rows display pressure waveforms measured under the far-neck [Fig. 2(a)] and near-neck [Fig. 2(b)] occiput regions. Inner pressure in each tube changes in accordance with respiratory motion and cardiac beating. The lower two rows are FPP [Fig. 2(c)] and nasal thermistor waveforms [Fig. 2(d)], respectively. It can be seen that spike-like pulses appeared in the far-neck and near-neck occiput pressures and the variations are beat-by-beat quite synchronous with the heartbeats in the FPP signal. However, heart pulses in the near-neck signal are much more distinguishable than those in the far-neck signal. In contrast, the respiration rhythm in both pressure signals [Fig. 2(a) and (b)] can be identified clearly breath-by-breath, corresponding to the nasal thermistor signal, although slight misalignments in phase exist between different signals. Based upon these observations, the near-neck pressure signal was used in the detection for the respiration rhythm and pulse rate.

B. Subjects

The near-neck and far-neck occiput pressure signals were collected from 13 healthy subjects (5 female and 8 male fourth-year college students, 21–22 years of age) at the School of Health Sciences, Kanazawa University, Japan. Approximately 2 hr. data were recorded from each subject during sleep. Finger photoelectric plethysmography and nasal thermistor signals were also collected as references for the pulse rate and respiration rhythm, respectively.

C. à Trous-Based Wavelet Transformation

The WT can separate a signal into different components with wavelet functions derived by dilating and translating a single prototype wavelet function ψ [23]. The WT of a signal f is defined as

$$W_s f(a) = \frac{1}{\sqrt{s}} \int_{-\infty}^{+\infty} f(t)\psi\left(\frac{t-a}{s}\right)dt \tag{1}$$

where s and a are the scale and translation factors of the prototype wavelet ψ, respectively. The translation factor a is a parameter to observe the whole signal through shifting the compact supported wavelet function at a specific time. When the scale factor s is altered from small to large, the basis wavelet function is dilated in the time domain and the corresponding WT coefficients give rougher representation of a signal in the lower frequency range, and *vice versa.*

When a discrete signal f, sampled at a regular interval T, is taken into consideration, the scale factor s and the translation factor a can be discretized on a dyadic grid plane: $s = 2^j$, $a = 2^j k$, where j, $k \in$ Z and Z is the integral set. This kind of the WT is called a dyadic WT (DWT). Its basis functions are expressed as

$$\psi_{j,k}(t) = 2^{-j/2}\psi(2^{-j}t - k), j, k \in \mathrm{Z}. \tag{2}$$

To realize multiple decomposition of a discrete signal at different scales, a recursive Mallat's algorithm can be applied as a cascade of a highpass FIR filter g_0 and a lowpass FIR filter h_0 in each scale [23], as illustrated in Fig. 3(a). g_0 is the high-pass filter to obtain the detail component; and h_0 is the low-pass filter to obtain the approximation component. $H_0(z)$ and $G_0(z)$ are the Z transformation of h_0 and g_0. The raw signal is decomposed into the approximation (a_j) and detail (d_j) components. However, Mallat's algorithm includes the subsampling procedure after each filtering step; and this manipulation leads to the signal phase variant (time shifting) and reduces the temporal resolution of wavelet coefficients as the scale increases [23], [26]. Real-time application requires an efficient implementation that does not lead to deterioration of detection accuracy. One idea was to decompose the signal into the approximation (a'_j) and detail (d'_j) components at the same sampling rate in all scales by neglecting the decimation processing. This can be achieved by using the *à trous* algorithm [24] as shown in Fig. 3(b). The *à trous* algorithm is one of the possible alternatives to maintain the consistency in the signal phase and the temporal resolution at different scales. It has almost the same structure as the Mallat's

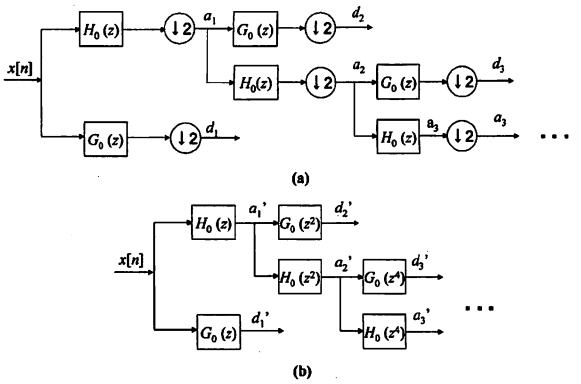


Fig. 3. The DWT cascade structures of (a) Mallat's algorithm and (b) *à trous* algorithm. See the text for details.

algorithm except for the subsampling procedure. However, unlike Mallat's algorithm, the *à trous* algorithm is time-invariant and has the same temporal resolution in every scale [26]. The *à trous* algorithm neglects the down-sampling and up-sampling procedures and its equivalent low- and highpass filters in the $s = 2^j$ scale are replaced by $H_0(z^s)$ and $G_0(z^s)$ [24].

When ψ is a symmetric function, the discrete Fourier transform (DFT) of the DWT is [23]

$$\begin{aligned}&\mathrm{DFT}(W_{2^j} f(n))\\ &= \mathrm{DFT}(f(n))\mathrm{DFT}(\psi_{2^j}(n)) = F(\omega)\,\Psi\left(2^j\omega\right)\\ &= \begin{cases} G_0(\omega)F(\omega)\Phi(\omega) & j=1\\ G_0(2\omega)H_0(\omega)F(\omega)\Phi(\omega) & j=2\\ G_0\left(2^{j-1}\omega\right)H_0\left(2^{j-2}\omega\right)\ldots H_0(\omega)F(\omega)\Phi(\omega) & j>2\end{cases}\end{aligned} \tag{3}$$

where $\Phi(\omega)$ is the DFT of a smoothing function φ, $G_0(\omega)$ and $H_0(\omega)$ are the Fourier transformation of the highpass filter g_0 and lowpass filter h_0 in the filter bank, respectively, and $F(\omega)\Phi(\omega)$ is the discrete Fourier transformation of the pressure signal $x[n]$.

From (3), the WT of $x[n]$ at scale 2^j is equivalent to filtering $x[n]$ through G_0 and H_0. The frequency responses $Q_j(\omega)$ and $P_j(\omega)$ of the equivalent filter for the detail and approximation components at scale 2^j are

$$Q_j(\omega) = \begin{cases} G_0(\omega) & j=1\\ G_0\left(2^{j-1}\omega\right)\prod_{l=0}^{j-2} H_0\left(2^l\omega\right) & j>1\end{cases} \tag{4}$$

$$\text{and } P_j(\omega) = \begin{cases} H_0(\omega) & j=1\\ \prod_{l=0}^{j-1} H_0\left(2^l\omega\right) & j>1\end{cases}. \tag{5}$$

Here, the *à trous* algorithm is used to extract the respiration- and pulse-related waveforms from the occiput pressure signals only through the decomposition procedure. The CDF (Cohen-Daubechies-Fauraue) (9,7) biorthogonal wavelet is selected as the prototype wavelet to design the decomposition and reconstruction filters [27]; it has compact support and four vanishing moments. The coefficients of the decomposition filters are shown in Table I. As the filters are symmetrical with a linear phase shift [27], the time delay in outputs of the equivalent filters can be easily estimated and adjusted with respect to the raw signal in the real-time processing.

TABLE I
COEFFICIENTS OF DECOMPOSITION FILTERS USED IN DWT

n	$g_0[n]$	$h_0[n]$
0	0	0
1	-0.04563588155695	0.02674875741100
2	0.02877176311397	-0.01686411844300
3	0.29563588155670	-0.07822326652900
4	-0.55754352622844	0.26686411844300
5	0.29563588155670	0.60294901823600
6	0.02877176311397	0.26686411844300
7	-0.04563588155695	-0.07822326652900
8	0	-0.01686411844300
9	0	0.02674875741100

D. Real-Time Solution

Real time implementation for detection of respiration rhythm and pulse rate during sleep is shown in Fig. 4. Pressure signals were acquired through a 16-bit A/D card at 100 Hz sampling rate and buffered into a ring memory. In order to maintain continuity of the digital filtering procedure, once every 10 s (adjustable) the data frame was buffered, the newly formed 10-s data frame was decomposed into details and approximations by multiresolution WT based-upon the *à trous* algorithm. Therefore, the 2^k scale components will become $10+m_k$ s, where m_k is the extra part introduced by digital filtering. The whole 2^k scale components can be catenated together with the overlap-add method. After removing noise in the detail components in the 2^4 and 2^5 scales by a soft-threshold method, they are combined to form a pulse-related waveform. The approximation component in the 2^6 scale is used as a respiration-related waveform. Because all the filters are symmetrical with a linear phase shift, the latency for each component is $m_k/2$. The detail components of the 2^4 and 2^5 scales can be summed by setting $m_4/2$ and $m_5/2$ as the respective start times. Respiration rhythm and pulse rate readings are updated every 10 s following the recommendation of ANSI/AAMI EC13 [30]. In fact, the updating interval can be set to any feasible value in practical application.

The two main procedures in the real-time implementation are the *à trous* algorithm-based WT for waveform extraction of relevant components, and an adaptive characteristic point pursuit for characteristic point determination. The following describes more details on the real-time implementation of relevant waveform extraction and characteristic point detection.

E. Determination of the Characteristic Scales for Estimating Respiration and Pulse Waveforms

To determine the proper scales, by which respiration- and pulse-related waveforms can be estimated, we have to understand the properties of the respiration- and pulse-related signals as well as the characteristics of the equivalent digital filters $Q_j(\omega)$ and $P_j(\omega)$ of the selected DWT.

Corresponding to a sampling rate of 100 Hz, the 3-dB bandwidths of the equivalent filters $Q_j(\omega)$ and $P_j(\omega)$ in the different scales are tabulated in Table II. Although portions of the passbands among the different scales overlap, there is a distinct central frequency in each scale. The central frequency ranges, within which the most energy of the respiration and pulse-related waveforms are concentrated, were examined using

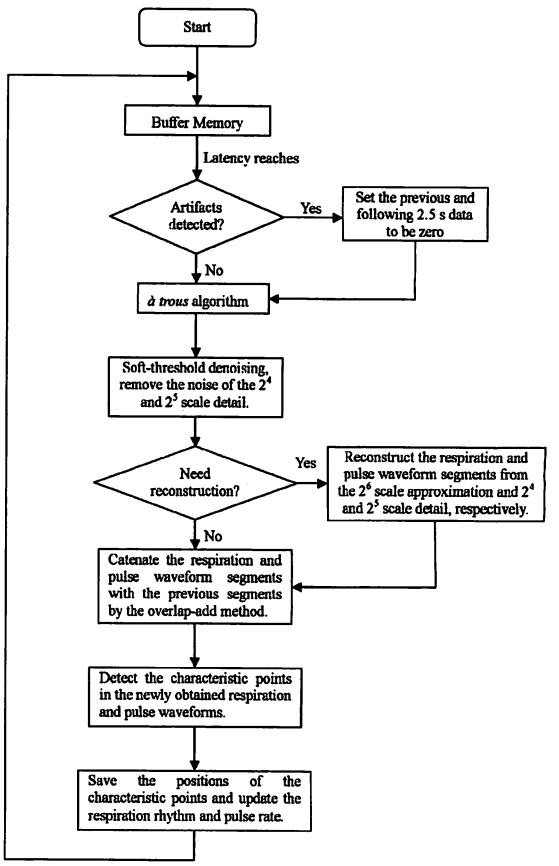


Fig. 4. Flowchart showing the real-time processing steps.

power spectra density (PSD) analysis with the Welch's method. A 4096–point segment of raw signal, 40.96 s in length, free of artifacts, was selected to evaluate the reasonable frequency ranges for the respiration and pulse-related waveforms. A Hanning window of 512-point width and 1024-point fast Fourier transform was used. Fig. 5 shows the frequency spectrum of the raw signal segment illustrated in Fig. 2(b). The PSD peak at 0.293 Hz corresponds to the respiration rhythm, which is equivalent to 17.6 breaths/min, the result estimated from the reference signal, as shown in Fig. 2(d). The PSD peak at 1.270 Hz is relevant to the pulse rate, which is equivalent to 77.6 beats/min, the result estimated from the reference signal, as shown in Fig. 2(c). Other PSD peaks at 2.637, 3.906, 5.176, and 6.445 Hz indicate the harmonic components of the pulse-related waveform in the raw pressure signal. Similar results can be found in the data from other subjects. From Fig. 5 and a general understanding of respiration and the heartbeat, it can be concluded that the proper frequency range for the respiration-related waveform is within 0.1–0.5 Hz, and 0.6–6.0 Hz for the pulse-related waveform. It was observed that most of the spectral energies in the respiration-related signal are included in the approximation component of the 2^6 scale; and the spectral range in the pulse-related signal appears to extend across more than one scale, and may contain a significant portion of the detail components of the 2^4 and 2^5 scales. Although the 2^6 scale detail component occupies the frequency range 0.8–1.7 Hz, in this frequency range the pulse wave appears to be the sinus wave not the pulse peak. Therefore, we

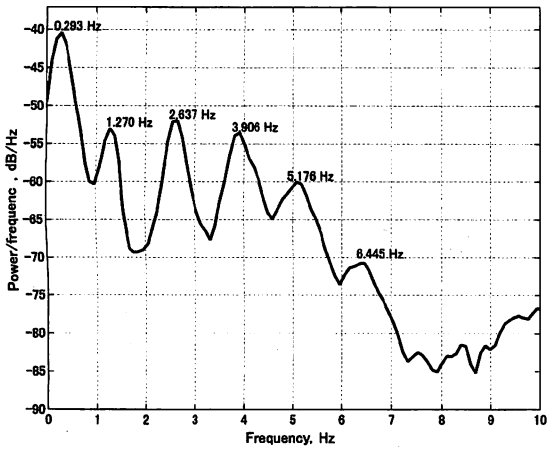


Fig. 5. The PSD of the near-neck occiput pressure signal. The leftmost peak is corresponding to the respiration rhythm. Its next peak is a fundamental frequency of heartbeats. Other peaks are the harmonics of the heartbeats.

TABLE II
THREE-DECIBEL BANDWIDTHS OF EQUIVALENT DIGITAL FILTERS $Q_j(\omega)$ AND $P_j(\omega)$ IN THE 2^1–2^6 SCALES WITH RESPECT TO THE SAMPLING RATE OF 100 HZ

Scale, 2^j	$Q_j(\omega)$ 3 dB Bandwidth (Hz)	$P_j(\omega)$ 3 dB Bandwidth (Hz)
2^1	26.7–50.0	0–27.3
2^2	13.6–27.8	0–13.3
2^3	6.7–13.9	0–6.5
2^4	3.4–6.9	0–3.3
2^5	1.7–3.3	0–1.7
2^6	0.8–1.7	0–0.8

do not use the 2^6 scale detail to synthesize the pulse-related waveform.

F. Determination of the Characteristic Scales for Estimating Respiration and Pulse Waveforms

Fig. 6 shows the raw signal of the pulsatile pressure measured in the near-neck occiput [Fig. 6(a)], and its DWT decomposed waveforms [Fig. 6(b)–(h)]. The time delay after convolution with each WT filter is removed from the decomposed component in every scale for illustration. The raw signal shown in Fig. 6(a) is the same as in Fig. 2(b). The detail components in the 2^1–2^6 scales are shown in Fig. 6(b)–(g). Fig. 6(h) shows the approximation component in the 2^6 scale. It was found that the approximation component in the 2^6 scale corresponds well with the respiration reference, i.e., the nasal thermistor signal in Fig. 2(d). The waveform reconstructed from the detail components in the 2^4 and 2^5 scales contains the most similar pulse-like peaks corresponding to the reference waveform measured by the FPP shown in Fig. 2(c). These results confirmed our observation and analysis that the approximation component in the 2^6 scale can be used to estimate the respiration-related waveform, and the detail components in the 2^4 and 2^5 scales can be used to estimate the pulse-related waveform after applying the soft-threshold method to remove noise [25].

In order to realize real-time application, both the respiration and pulse-related waveforms are obtained while neglecting the reconstruction procedure in the *à trous* algorithm. That is, the

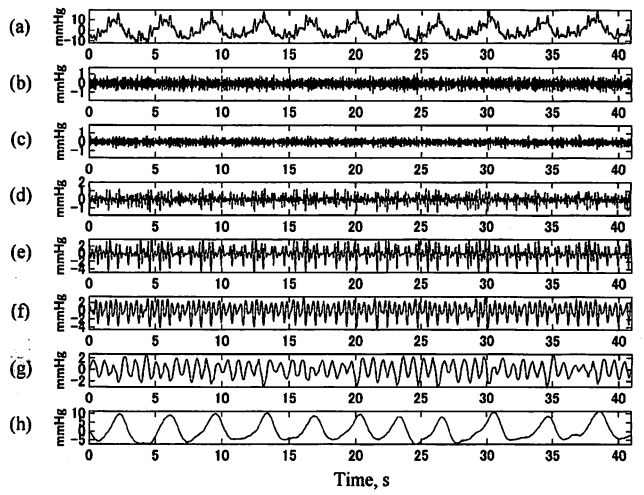


Fig. 6. The DWT decompositions of pressure signal detected with the sensor in near-neck occiput region. (a) the raw signal; (b)–(g) the waveforms of the detail components at the 2^1–2^6 scales, respectively; (h) the waveform of the approximation component at the 2^6 scale.

approximation in the 2^6 scale is used to represent the respiration-related waveform straightly, and summing the detail components of the 2^4 and 2^5 scales after denoising gives the pulse-related waveform. However, when the details in the 2^4 and 2^5 scales are added together directly, special attention should be paid to the difference in time shift between the two waveforms after the convolution operation. We should take away the extra time-shift in the detail component of the 2^5 scale before adding it to the detail component of the 2^4 scale. In addition, for the method without the reconstruction procedure, the 2^4 and 2^5 scales are multiplied with -1 to get the pulse-related waveform in this paper because upward peaks in the raw signal will be inverted by the high pass filter g_0 in Table I.

G. Detection of Pulse Rate and Respiration Rhythm

The algorithm for detecting the pulse rate from either the FPP or the estimated pulse-related waveform is an adaptive pulse peak pursuit method refined from the ECG R-wave detection algorithm in Pan *et al.* [28]. The adaptive pulse peak pursuit algorithm is described below.

The input signal is first processed through a first-derivative operator, and then points corresponding to the pulse peaks are determined by the characteristic point search algorithm with a locally adaptive threshold. The initial pulse detection threshold is set to be 70% of the average value of the five largest first-derivatives in the first 5 s data segment. When a point with a value over the threshold is found in the differential data, the peak point with a local maximum value around it in the input signal is set to be the pulse characteristic (peak) point. When a period without finding a pulse peak point is over 1.8 times the previous characteristic point interval, the threshold will be reduced 50% and the search procedure restarts. After each pulse peak is detected, the threshold will be updated to the previous threshold multiplied by 0.7 + the current largest first derivative multiplied by 0.3 * 0.7. A refractory time of 180 ms is set to avoid analyzing the data after the pulse characteristic point.

The characteristic points for detecting respiration rhythm from the nasal thermistor signal and estimated respiration-related waveform are defined as the upward zero-cross points in the input waveforms. The zero line is locally adapted to track the wandering baseline. The initial zero-line value is selected as the average value of the first 5 s data; and updated to be the previous zero-line value multiplied by 0.7 + the average of the preceding 5 s data multiplied by 0.3 when a new zero-cross point is found. Only the upward zero-cross points with preceding valleys lower than the valley threshold are recognized as qualified characteristic points. The initial valley threshold is set to be the 0.2 time of the standard deviation of the first 5 s data, and is updated to the previous valley threshold multiplied by 0.7 + the standard deviation of the preceding 5 s data multiplied by $0.3 * 0.2$ when a new qualified characteristic point is found. A refractory time of 500 ms is set to avoid analyzing the data behind the qualified zero-cross characteristic point. The coefficients for the detection of respiration rhythm and pulse rate are determined empirically.

Before detection of the characteristic points, artifacts in the pressure signal caused by body movements are detected using a threshold method. When an extremely large value, whose absolute value is 4 times larger than the standard deviation of the preceding detected artifact-free raw signal, is found in the raw pressure signal, the preceding and succeeding 2.5-s raw pressure signals are neglected and not used for the estimation of respiration rhythm and pulse rate. In summary, real-time detections of the respiration rhythm and pulse rate are realized by the following steps:

1) Processing a definite n s duration (e.g., 10 s) signal segment sequentially with an *à trous* algorithm-based DWT.
2) Each estimated waveform segment is catenated to the previous one with an overlap-add method to create a complete waveform.
3) The detail components in the 2^4 and 2^5 scales are realigned in the signal phase and summed in amplitude as an estimation of the pulse-related waveform.
4) The approximation component in the 2^6 scale serves as the estimation of the respiration-related waveform.
5) When artifacts due to exorbitant movements are detected, the preceding and succeeding 2.5 s signal segment will be neglected in analysis.
6) The complete waveform is used to detect the characteristic points for the respiration rhythm and the pulse rate by the adaptive characteristic point pursuit method.

To compare the performance between the methods with and without reconstruction, the DWT with reconstruction procedure is also evaluated. The reconstruction filters H_1 and G_1 can be derived from the decomposition filters, i.e., $H_1(z) = -G_0(-z)$ and $G_1(z) = H_0(-z)$ [27]. It is clear that all of the filters are symmetrical or anti-symmetrical and have a linear phase property. Therefore, the time delay can be accurately estimated and handled properly in the real-time processing. The detail of the reconstruction procedure of DWT can be found in [27].

Fig. 7 demonstrates, from top to bottom, the raw pressure signal measured under the near-neck occiput [Fig. 7(a)]; the FPP signal [Fig. 7(b)]; the estimated pulse-related waveform with [Fig. 7(c)] and without [Fig. 7(d)] reconstruction; the nasal thermistor signal [Fig. 7(e)]; and the estimated respiration-related waveform with [Fig. 7(f)] and without [Fig. 7(g)] reconstruction. The detected characteristic points are marked by a black dot "•." It can be seen from Fig. 7 that the pulse and respiration-related waveforms estimated with and without reconstruction procedures are very similar in morphology. This fact implies that the detail and approximation components can be used directly as the pulse and respiration-related waveforms.

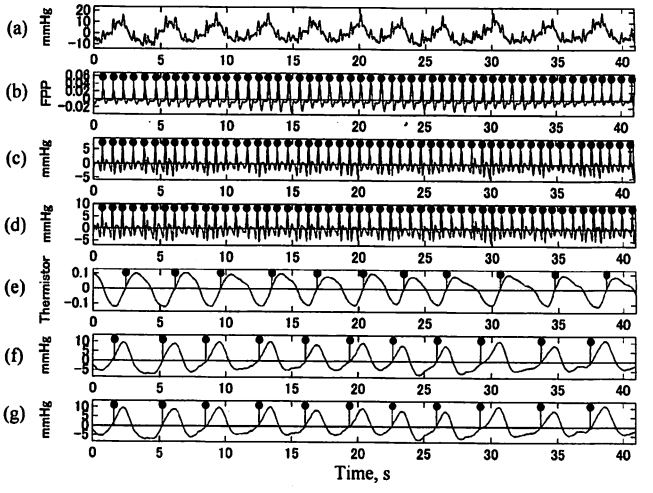


Fig. 7. Estimated signals and detected characteristic points (indicated by "•"). (a) the raw signal; (b) FPP; (c) the estimated pulse-related waveform with reconstruction procedures; (d) the estimated pulse-related waveform without reconstruction procedures; (e) the nasal thermistor signal; (f) the estimated respiration-related waveform with reconstruction procedures; and (g) the estimated respiration-related waveform without reconstruction procedures.

H. Performance Evaluation of Detection

From Fig. 7, it is clearly identified that the characteristic points in the pulse rate detection, from either reference [Fig. 7(b)] or estimated waveforms [Fig. 7(c) and (d)], synchronize beat-by-beat. Similar results in respiration rhythm detection can be seen in Fig. 7(e)-(g) based on breath-by-breath.

To evaluate the detection performance of the pulse rate and the respiration rhythm, a method is proposed and described as follows.

1) Counting the number of detected peaks in the FPP and the estimated pulse-related waveform within each minute free of artifacts as the real pulse beat number (RPBN) and the estimated pulse beat number (EPBN), respectively. It should be noticed that the RPBN is not always equal to the EPBN because of misdetection.
2) For each minute, when the EPBN is bigger than the RPBN, the false positive number (FPN) is EPBN–RPBN. Summation of all FPNs gives the total false positive number (TFPN). Similarly, for each minute when the EPBN is smaller than the RPBN, the false negative number (FNN) is RPBN–EPBN. Summation of all FNNs gives the total false negative number (TFNN).
3) Summation of all RPBNs gives the total real pulse beat number (TRBN). Summation of all EPBNs gives the total estimated pulse beat number (TEBN). The total true positive number (TTPN) equals TEPN–TFPN.

TABLE III
PULSE BEAT DETECTION RESULTS FROM FPP AND ESTIMATED PULSE-RELATED WAVEFORMS

Subject ID.	Data length (min)	Number of heart beats detected by			*PFNR* (%)		*PFPR* (%)		*PSe* (%)		*PP*$^+$ (%)	
		FPP	A	B	A	B	A	B	A	B	A	B
1	131.7	7409	7508	7423	1.82	2.93	3.16	3.12	98.21	97.15	96.94	96.97
2	133.4	9268	9248	9254	0.58	0.66	0.37	0.51	99.42	99.34	99.63	99.49
3	66.7	4719	4739	4737	0.21	0.47	0.64	0.85	99.79	99.53	99.36	99.16
4	48.3	2813	2862	2868	0.04	0.00	1.78	1.96	99.96	100.00	98.25	98.08
5	66.7	3681	3701	3703	0.16	0.22	0.71	0.82	99.84	99.78	99.30	99.19
6	133.4	6843	6855	6817	0.06	1.14	0.77	0.76	99.94	98.87	99.24	99.25
7	100.0	4901	4958	4935	1.98	2.14	3.14	2.84	98.06	97.90	96.96	97.24
8	266.0	17484	17726	17723	0.50	0.59	1.88	1.96	99.50	99.41	98.15	98.08
9	133.4	9046	9080	9090	0.93	1.06	1.31	1.55	99.08	98.95	98.71	98.47
10	128.7	6031	6129	6144	0.36	0.38	1.99	2.26	99.64	99.62	98.05	97.79
11	66.7	5158	4937	4908	4.81	5.49	0.52	0.64	95.41	94.80	99.48	99.36
12	33.3	1934	1970	1963	0.00	0.00	1.86	1.50	100.00	100.00	98.17	98.52
13	186.7	11529	11663	11646	0.16	0.17	1.33	1.19	99.84	99.83	98.69	98.82
AVG	—	—	—	—	0.89	1.12	1.50	1.55	99.17	98.91	98.53	98.47
STD	—	—	—	—	1.11	1.32	0.85	0.79	1.08	1.26	0.82	0.77
Total	1495.0	90816	91376	92070	—	—	—	—	—	—	—	—

Weighted average, weighted by the number of pulse beats per case.

A: the pulse-related waveform estimated without the reconstruction procedure

B: the pulse-related waveform estimated with the reconstruction procedure

4) The pulse false positive rate (PFPR), pulse false negative rate (PFNR), pulse sensitivity (PSe), and pulse positive predictivity (PP^+) are calculated as

$$\mathrm{PFPR} = \frac{\mathrm{TFPN}}{\mathrm{TRBN}} \times 100(\%) \tag{6}$$

$$\mathrm{PFNR} = \frac{\mathrm{TFNN}}{\mathrm{TRBN}} \times 100(\%) \tag{7}$$

$$\mathrm{PSe} = \frac{\mathrm{TTPN}}{(\mathrm{TTPN} + \mathrm{TFNN})} \times 100(\%) \tag{8}$$

and

$$\mathrm{PP}^+ = \frac{\mathrm{TTPN}}{(\mathrm{TTPN} + \mathrm{TFPN})} \times 100(\%). \tag{9}$$

5) Similar principles are applied to the respiration rhythm detection. They are

$$\mathrm{RFPR} = \frac{\mathrm{TFPN}}{\mathrm{TRRN}} \times 100(\%) \tag{10}$$

$$\mathrm{RFNR} = \frac{\mathrm{TFNN}}{\mathrm{TRRN}} \times 100(\%) \tag{11}$$

$$\mathrm{RSe} = \frac{\mathrm{TTPN}}{(\mathrm{TTRN} + \mathrm{TFNN})} \times 100(\%) \tag{12}$$

and

$$\mathrm{RP}^+ = \frac{\mathrm{TTPN}}{(\mathrm{TTRN} + \mathrm{TFPN})} \times 100(\%) \tag{13}$$

where TRRN is the total real respiration number, TERN is the total estimated respiration number, TTPN is the total true positive number. RFPR is the respiration false positive rate, RFNR is the respiration false negative rate, RSe is the respiration sensitivity, and RP^+ is the respiration positive predictivity. It should be noticed that when artifacts are found in the pressure signal, the pulse rate and respiration rhythm will not be estimated at that moment.

III. RESULTS

The results of the evaluation of pulse beat detection from the FPP and estimated signals are tabulated in Table III. The analyzed data were collected from 13 subjects, and the total time was about 24 hours. The total pulse beat number from the FPP signals at the time when the pressure signals were free of artifacts according to the artifact detection algorithm was 90816. Without the reconstruction procedure, PSe and PP^+ were $99.17\% \pm 1.08\%$ and $98.53\% \pm 0.82\%$, respectively. With the reconstruction procedure, the corresponding outcomes were $98.91\% \pm 1.26\%$ and $98.47\% \pm 0.77\%$, respectively.

Table IV summarizes the results of evaluation of respiration detection from the nasal thermistor and estimated signals. The analyzed data are the same as those in Table III. The total number of breaths from the nasal thermistor signal at the time when the pressure signals were free of artifacts was 23086. Without the reconstruction procedure, RSe and RP^+ were $95.63\% \pm 2.71\%$ and $95.42\% \pm 3.77\%$, respectively. With the reconstruction procedure, they were $94.76\% \pm 3.38\%$ and $96.92\% \pm 2.95\%$, respectively.

Fig. 8 shows a 64 min profile of estimated results and relative errors from the derived waveforms without reconstruction procedures. The real respiration rhythm (RRR, marked with "×") from the nasal thermistor, and the respiration rhythms estimated from the estimated respiration-related waveform (ERR, marked with "o" for periods without artifacts, without "o" for periods with artifacts) are shown in Fig. 8(a). The relative percentage of estimation errors, derived as $(\mathrm{ERR} - \mathrm{RRR})/\mathrm{RRR} \times 100(\%)$, is shown in Fig. 8(b). Fig. 8(c) shows the real pulse rate (RPR, marked with "×") from the FPP, and the pulse rate estimated from the estimated pulse-related waveform (EPR, marked with "o"for periods without artifacts, and without "o" for periods with artifacts). Fig. 8(d) shows the relative percentage of estimation errors, derived as $(\mathrm{EPR} - \mathrm{RPR})/\mathrm{RPR} \times 100(\%)$. It can be seen that most of the errors for the pulse rate and respiration rhythm are within a range of $\pm 10\%$.

IV. DISCUSSIONS

Watanabe *et al.* proposed a digital filtering method to extract desired waveforms from measured near-neck occiput pressure

TABLE IV
RESPIRATION DETECTION RESULTS FROM THE NASAL THERMISTOR AND THE RESPIRATION-RELATED WAVEFORMS

Subject ID.	Data length (min)	Number of breaths detected by Thermistor	A	B	*RFNR* (%) A	B	*RFPR* (%) A	B	*RSe* (%) A	B	*RP*$^+$ (%) A	B
1	131.7	1601	1786	1729	5.44	5.93	16.99	13.93	94.84	94.40	85.48	87.77
2	133.4	2456	2395	2394	2.77	2.81	0.29	0.28	97.30	97.27	99.71	99.72
3	66.7	1014	911	915	11.34	10.85	1.18	1.08	89.82	90.21	98.83	98.93
4	48.3	919	781	735	15.56	20.35	0.54	0.33	86.54	83.09	99.46	99.67
5	66.7	906	923	917	1.21	1.43	3.09	2.65	98.80	98.59	97.00	97.42
6	133.4	1921	1913	1900	3.49	3.96	3.07	2.86	96.63	96.19	97.02	97.22
7	100.0	1382	1349	1339	3.33	3.62	0.94	0.51	96.78	96.51	99.07	99.49
8	266.0	3853	3874	3825	3.01	3.22	3.55	2.49	97.08	96.88	96.57	97.57
9	133.4	2157	2151	2046	6.72	9.23	6.44	4.08	93.70	91.55	93.95	96.08
10	128.7	2244	2374	2284	1.20	1.78	7.00	3.56	98.81	98.25	93.46	96.56
11	66.7	770	748	744	5.32	5.32	2.47	1.95	94.95	94.95	97.59	98.09
12	33.3	604	567	519	10.93	16.56	4.80	2.48	90.15	85.79	95.42	97.58
13	186.7	3202	3337	3092	4.00	6.65	8.21	3.22	96.15	93.76	92.41	96.88
AVG	—	—	—	—	4.60	5.72	4.98	3.15	95.63	94.76	95.42	96.92
STD	—	—	—	—	3.12	4.02	4.38	3.38	2.71	3.38	3.77	2.95
Total	1495.0	23086	22461	23164	—	—	—	—	—	—	—	—

Weighted average, weighted by the number of breaths per case.

A: the respiration-related waveform estimated without the reconstruction procedure

B: the respiration-related waveform estimated with the reconstruction procedure

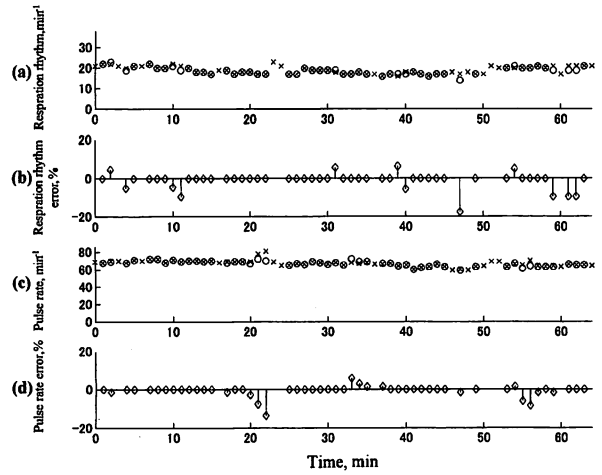


Fig. 8. Instantaneous profiles of (a) respiration rhythm and (c) pulse rate detected from the estimated waveforms (o) and the reference data (×); and estimation errors of (b) respiration rhythm and (d) pulse rate. "o" indicates that the value was detected when there was no artifact in that minute.

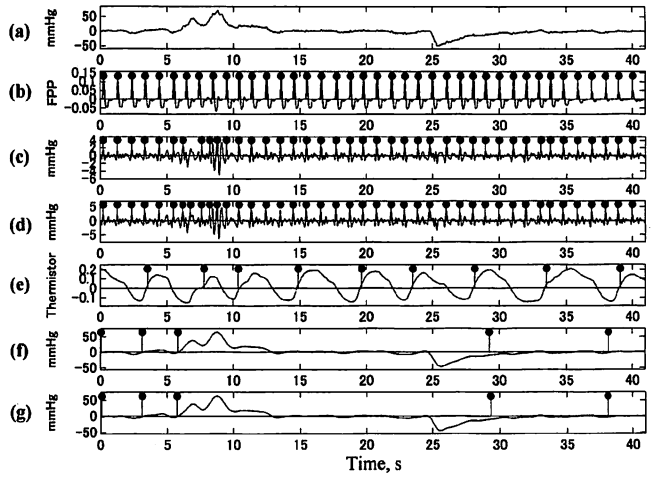


Fig. 9. Estimation results, including estimated waveforms and detected characteristic points in the case of poor signal quality. (a) the raw signal; (b) FPP; (c) the estimated pulse-related waveform with reconstruction procedures; (d) the estimated pulse-related waveform without reconstruction procedures; (e) the nasal thermistor signal; (f) the estimated respiration-related waveform with reconstruction procedures; and (g) the estimated respiration-related waveform without reconstruction procedures.

signals [14]. The raw signal passed through a bandpass filter (0.1–0.8 Hz) could be used to represent the respiration waveform, and the pulse rate was directly estimated from the peaks of the near-neck occiput pressure signal. However, such a narrow bandwidth filter in a low frequency band requires high order implementation and is not suitable for real-time application. On the other hand, when we use a bandpass filter to detect the pulse rate, the bandpass filter should have a rather wider bandwidth to cover the frequency range of the pulse wave about 0.67–5 Hz for 40–300 bpm. Therefore, the respiration-related component and random noise in the occiput pressure signal may mask the pulse signal and affect the detection of the pulse rate. Moreover, spectral overlapping in the frequency domain makes it difficult to discriminate the measurement noise and pulse-related signal using traditional filters. These would lead to false detection in the characteristic points, and increase the false negative or/and false positive rates. The PSD method cannot realize beat-by-beat analysis and fails when the signal/noise ratio is too low or the respiration rhythm and pulse rate is closer than the highest frequency resolution of the PSD. According to [30], the minimum data length for cardiac rate should be less than 10 s. For a N = 1000-point Hanning window and f_s = 100 Hz sampling rate, the highest frequency resolution of PSD is about $4f_s/N = 4 \times 100/1000 = 0.4$ Hz. Increasing the point count of the window function will reduce the temporal resolution of the PSD although its frequency resolution can be raised. The method proposed in this paper overcomes this issue to some extent. Fig. 9 shows the detection results in a typical situation where artifact appears, illustrating the raw pressure signal

[Fig. 9(a), the FPP [Fig. 9(b)], the estimated pulse-related waveforms with reconstruction procedure [Fig. 9(c)], without reconstruction procedure [[Fig. 9(d)], the nasal thermistor [Fig. 9(e)], the estimated respiration-related waveforms with reconstruction procedure [Fig. 9(f)], and without reconstruction procedure [Fig. 9(g)]. It is clear that the pulse-related waveform can be estimated by the method proposed in this paper. However, artifacts greatly worsen estimation of the respiration rhythm. Such artifacts might be one reason why the detection accuracy of the pulse rate is better than that of the respiration rhythm. This means that the proposed method is much more robust for pulse rate detection than for respiration rhythm detection.

It can be seen from Fig. 2(a) and (b) that there is a phase difference in the respiration-related waveforms between the near-neck and far-neck occiput pressures. Because pressure variations due to the breathing movement and heartbeat pulsation reach two measurement sites—i.e., the far-neck and near-neck—via two different transmission routes, this implies that a simple additive model is not accurate enough to describe the relation between the far-neck and near-neck pressure variations. This phenomenon leads to dissatisfaction with the instant mixing requirement in the linear ICA model [29] and, therefore, to incomplete separation of the pulse and respiration waveforms [15].

Because the DWT performs as a bank of bandpass filters [23], this feature is successfully used to separate signals into different frequency components. It is well known that the fundamental frequencies of the respiration rhythm and pulse rate are located in different frequency bands. Through the DWT decomposition, the respiration- and pulse-related waveforms can be both estimated from the measured pressure signal.

In contrast to the ICA method, [29] the DWT approach can estimate the respiration and pulse-related waveforms from only one pressure signal channel. In addition, unlike the time-consuming recursive optimization calculation used in the ICA method, the computational complexity of the proposed method can be greatly reduced because only the characteristic scales need to be decomposed. From Tables III–IV, it is found that the detection performances for the pulse and respiration-related waveforms, estimated with and without reconstruction, are very close. From one-way analysis of variance, the significance levels P between the performance indexes for reconstruction and nonreconstruction are much larger than 0. It can be concluded that there is little deterioration in the detection performance even when the pulse and respiration-related waveforms are estimated without the DWT reconstruction procedure. This leads to improved real-time processing efficiency. Moreover, the avoidance of subsampling procedure by using the *à trous* algorithm [24] also assures phase shift invariance, which means that the algorithm can be easily implemented using any digital signal processor in real world applications.

It should be noticed that the evaluation results depend on the selection of the coefficients of the threshold for the detection of characteristic points. The coefficients used in this paper were decided empirically to obtain a proper combination of Se and P^+. From Table III, it can be observed that the PFNR is lower than the PFPR for the pulse rates of most subjects with or without the reconstruction procedure. This implies that most of the estimates tend to be larger in value than the reference data, and that few estimates have lower readings of pulse rate than the reference data when these coefficients are selected. From Table IV, it is found that the method with reconstruction procedure tends to detect more respiration than that without reconstruction procedure does. The reconstruction procedure may raise the positive predictivity while reducing the sensitivity of detection when these coefficients are selected.

Differences in detected timing of characteristic points between the reference and estimated signals can be identified in Fig. 7, especially between the nasal thermistor and the estimated respiration-related waveforms in Fig. 7(e)-(g). Because only the beat-by-beat or breath-by-breath readings are concerned, offset in the detected timing of characteristic points is not an exigent issue.

Three main sources of degraded detection performance are considered. One is the artifact induced by body movement. When a subject turns over in bed frequently during sleep, the measured pressure pattern distorts and the characteristic points for the respiration rhythm and pulse rate cannot be properly detected from the estimated waveforms. This fact can be found in Fig. 8, where the detection error increases when there were artifacts in the preceding or succeeding pressure signal. Usually the transition period lasts for about 2–3 s. It will especially influence the detection of respiration rhythms as shown in Fig. 9. However, we found that although it was hard to obtain signal satisfactory enough to analyze in the posture transition period, measured signals were acceptable provided the near-neck occipital region has good contact to the pillow for any sleep gestures. Furthermore, the amplitude of the pressure signal is not sensitive to the sleep gesture. In this paper, the artifacts due to the body movement were detected with the threshold method because the sensor usually detected a slow and large waveform at that time. In the data used in this research, only 5% data were found with artifacts due to body movement. If the artifact only lasts for a short time, the respiration rhythm and heart rate may be interpolated by using the preceding and succeeding values.

The second factor is the sensor signal drop-out. When the sensor plate is not correctly positioned beneath the pillow, pressure variations under the head cannot reach the sensor plate. It will severely influence the detection of respiration rhythm and pulse rate. This problem may be solved by binding the pillow tightly to the sensor plate.

The last factor is that the head may have no good contact with the pillow and the pressure variation cannot be transmitted to the sensor through the pillow. This problem should be resolved by improving the sensor mechanism and even system to achieve a larger dynamic measurement range.

Because only one pressure signal channel is used to estimate the respiration rhythm and pulse rate, the measurement instrument configuration is greatly simplified. In order to further improve detection performance, more robust algorithms, more reliable detection strategies, and structural fabrication for handling sensor signal drop-out and movement artifacts will be important. Furthermore, clinical data regarding various sleep disorders should be collected and assessments made of the accuracy and reliability of the proposed method in application as a sleep disease monitor.

V. Conclusion

A real-time processing method to estimate the respiration rhythm and the pulse rate from the occiput pressure signal, with noninvasive unconstrained measurements during sleep, was proposed and verified. The pressure signal was decomposed into detail and approximation components with the DWT multiresolution analysis method. The respiration rhythm can be detected from the approximation component in the 2^6 scale, and the pulse rate can be attained from the detail components in the 2^4 and 2^5 scales after noise suppression with the soft threshold method. The reconstruction procedure can even be neglected without deterioration of detection performance. This method provides an accurate and a reliable means to monitor the respiration rhythm and the pulse rate in real-time during sleep. After clinical evaluation and practical feasibility are studied, this method is expected to be applicable in the diagnosis of sleep apnea, sudden death syndrome, and arrhythmias during sleep.

Acknowledgment

The authors are grateful to students at the School of Health Sciences, Kanazawa University, for their efforts in data collection, and appreciate anonymous reviewers' valuable advices and encouragement to help polishing the paper.

References

[1] R. Wolk, A. S. Gami, A. Garcia-Touchard, and V. K. Somers, "Sleep and cardiovascular disease," *Curr. Probl. Cardiol.*, vol. 30, no. 12, pp. 625–662, Dec. 2005.

[2] T. L. Lee-Chiong Jr. and U. Magalang, "Monitoring respiration during sleep," *Respir. Care Clin. N. Am.*, vol. 11, no. 4, pp. 663–678, Dec. 2005.

[3] R. S. Leung, M. E. Bowman, T. M. Diep, G. Lorenzi-Filho, J. S. J. S. Floras, and T. D. Bradley, "Influence of Cheyne-Stokes respiration on ventricular response to atrial fibrillation in heart failure," *J. Appl. Physiol.*, vol. 99, no. 5, pp. 1689–1696, Jun. 2005.

[4] R. S. Leung, M. A. Huber, T. Rogge, N. Maimon, K. L. Chiu, and T. D. Bradley, "Association between atrial fibrillation and central sleep apnea," *Sleep*, vol. 28, no. 12, pp. 1543–1546, Dec. 2005.

[5] R. J. Thomas, J. E. Mietus, C. K. Peng, and A. L. Goldberger, "An electrocardiogram-based technique to assess cardiopulmonary coupling during sleep," *Sleep*, vol. 28, no. 9, pp. 1151–1161, Sep. 2005.

[6] M. R. Neuman, H. Watson, R. S. Mendenhall, J. T. Zoldak, J. M. Di Fiore, M. Peucker, T. M. Baird, D. H. Crowell, T. T. Hoppenbrouwers, D. Hufford, C. E. Hunt, M. J. Corwin, L. R. Tinsley, D. E. Weese-Mayer, and M. A. Sackner, "Cardiopulmonary monitoring at home: The CHIME monitor," *Physiol. Meas.*, vol. 22, no. 2, pp. 267–286, May 2001.

[7] L. G. Lindberg, H. Ugnell, and P. A. Oberg, "Monitoring of respiratory and heart rates using a fibre-optic sensor," *Med. Biol. Eng. Comput.*, vol. 30, no. 5, pp. 533–537, Sep. 1992.

[8] K. Nakajima, T. Tamura, and H. Miike, "Monitoring of heart and respiratory rates by photoplethysmography using a digital filtering technique," *Med. Eng. Phys.*, vol. 18, no. 5, pp. 365–372, Jul. 1996.

[9] G. Matthews, B. Sudduth, and M. Burrow, "A noncontact vital signs monitor," *Crit. Rev. Biomed. Eng.*, vol. 28, no. 1–2, pp. 173–178, 2000.

[10] G. B. Moody, R. G. Mark, A. Zoccola, and S. Mantero, "Derivation of respiratory signals from multi-lead ECGs," in *Proc. Computers in Cardiology*, 1985, vol. 12, pp. 113–116.

[11] P. de Chazal, C. Heneghan, E. Sheridan, R. Reilly, P. Nolan, and M. O'Malley, "Automated processing of the single-lead electrocardiogram for the detection of obstructive sleep apnoea," *IEEE Trans. Biomed. Eng.*, vol. 50, no. 6, pp. 686–696, Jun. 2003.

[12] D. Dobrev and I. Daskalov, "Two-electrode telemetric instrument for infant heart rate and apnea monitoring," *Med. Eng. Phys.*, vol. 20, no. 10, pp. 729–734, Dec. 1998.

[13] K. Nakajima, H. Yamakose, H. Kuno, M. Nambu, T. Irie, M. Higuchi, A. Sahashi, and T. Tamura, "A pillow-shaped respiration monitor," (in Japanese) *Life Support*, vol. 13, no. 1, pp. 2–7, Jan. 2001.

[14] K. Watanabe, T. Tasaki, T. Nemoto, K. Yamakoshi, and W. Chen, "Development of biometry system in the sleep by pillow cuff installed on the occiput," *Trans. Jpn. Soc. Med. Biol. Eng.*, vol. 41, suppl. 1, p. 168, 2003.

[15] M. Uchida, S. Ding, W. Chen, T. Nemoto, and D. Wei, "An approach for extractions of pulse and respiration information from pulsatile pressure signals," presented at the IEEE Asia-Pacific Biomed. Eng. Conf., Kyoto, Japan, Oct. 20–22, 2003.

[16] Y. Kanemitsu, Y. Yamashita, T. Nemoto, S. Takada, K. Kitamura, K. Yamakoshi, and W. Chen, "Development of biometry system in the sleep," presented at the 43rd Annual Conf. Japanese Society Med. Biol. Eng., Kanazawa, Japan, May 19–21, 2004.

[17] M. Akay, *Time Frequency and Wavelets in Biomedical Signal Processing*. Piscataway, NJ: IEEE Press, 1998.

[18] C. Li, C. Zheng, and C. Tai, "Detection of ECG characteristic points using wavelet transformation," *IEEE Trans. Biomed. Eng.*, vol. 42, pp. 21–28, Jan. 1995.

[19] M. L. Hilton, "Wavelet and wavelet packet compression of electrocardiograms," *IEEE Trans. Biomed. Eng.*, vol. 44, no. 5, pp. 394–402, May 1997.

[20] A. Khamene and S. Negahdaripour, "A new method for the extraction of fetal ECG from the composite abdominal signals," *IEEE Trans. Biomed. Eng.*, vol. 47, no. 4, pp. 507–516, Apr. 2000.

[21] J. P. Martinez, R. Almeida, S. Olmos, A. P. Rocha, and P. Laguna, "A wavelet-based ECG delineator: Evaluation on standard databases," *IEEE Trans. Biomed. Eng.*, vol. 51, no. 4, pp. 2464–2484, Apr. 2004.

[22] W. Chen, X. Zhu, T. Nemoto, Y. Kanemitsu, K. Kitamura, and K. Yamakoshi, "Unconstrained detection of respiration rhythm and pulse rate with one under-pillow sensor during sleep," *Med. Biol. Eng. Comput.*, vol. 43, no. 2, pp. 306–312, Mar. 2005.

[23] S. Mallat and S. Zhong, "Characterization of signals from multi-scale edges," *IEEE Trans. Pattern Anal. Mach. Intell.*, vol. 14, no. 7, pp. 710–732, Jul. 1992.

[24] M. Shensa, "The discrete wavelet transformation, wedding the *à trous* and the Mallat algorithm," *IEEE Trans. Signal Process.*, vol. 40, no. 10, pp. 2464–2484, Oct. 1992.

[25] C. Taswell, "The what, how, and why of wavelet shrinkage denoising," *Computing Sci. Eng.*, vol. 2, no. 3, pp. 12–19, May 2000.

[26] A. P. Bradley, "Shift-invariance in the discrete wavelet transforms," in *Proc. VIIth Digital Imaging Computing: Tech. and Appl.*, Sydney, Dec. 10–12, 2003, pp. 10–12.

[27] I. Daubechies, *Ten Lecture on Wavelets*. Philadelphia, PA: SIAM, 1992, p. 279.

[28] J. Pan and W. J. Tompkins, "A real-time QRS detection algorithm," *IEEE Trans. Biomed. Eng.*, vol. 32, no. 3, pp. 230–236, Mar. 1985.

[29] A. Hyvärinen, "Fast and robust fixed-point algorithms for independent component analysis," *IEEE Trans. Neural Netw.*, vol. 10, no. 3, pp. 626–634, May 1999.

[30] ANSI/AAMI EC13: Cardiac Monitors, Heart Rate Meters, and Alarms ANSI, 2002 [Online]. Available: http://webstore.ansi.org/ansidocstore/product.asp?sku=ANSI%2FAAMI+EC13-2002, 3rd



Xin Zhu (S'99) was born in Changsha, Hunan, China, in 1977. He received the B.S. and M.S. degrees in biomedical engineering from Tianjin University, Tianjin, China, in 2000 and 2002, respectively. He is now a doctoral candidate in the Graduate Department of Information Systems at the University of Aizu, Aizu-Wakamatsu, Fukushima, Japan. He received the Ph.D. degree in Information Systems from University of Aizu, Aizu-Wakamatsu, Fukushima, Japan in 2006.

He is now a postdoctoral researcher at University of Aizu. He has authored and co-authored over 30 journal and conference papers. He holds 1 patent and another one is under application. His research interests include biomedical modeling and simulation, biomedical signal and image processing, and bioinstrumentation.

Mr. Zhu is the recipient of the Second Prize of IEEE EMBS Japan Young Investigators Competition for EMBS2005 and the Third Prize of the student paper competition of IEEE EMBS APBME2000.



Wenxi Chen (M'02) received the B.Eng. and M.Eng. degrees both in biomedical engineering from Zhejiang University, Hangzhou, China, in 1983 and 1986, respectively, and the Ph.D. degree in medical science from Tokyo Medical and Dental University in 2001, Tokyo, Japan.

He had worked as a Research Engineer at the R&D center, Nihon Kohden Corporation, Japan, from 1992 to 1997. He is currently an Associate Professor at the Department of Computer Software, the University of Aizu, Aizu-Wakamatsu City, Japan. His research interests include biomedical signal processing, ubiquitous monitoring of vital signs, and the development of related technologies toward mobile phone applications in healthcare domain.

Dr. Chen is member of Japanese Society of Clinical Monitoring, Japanese Society for Biological and Medical Engineering, and the IEEE Engineering in Medicine and Biology Society (EMBS).



Tetsu Nemoto received the B.S. degree in electronic engineering from Nihon University, Tokyo, Japan in 1969. He received the Ph.D. degree in medical science from Tokyo Medical and Dental University in 1984.

From 1970 to 1987, he worked as a Technical Official at Tokyo Medical and Dental University. From 1987 to 1992, he was a Chief Researcher at the National Institute of Animal Industry. From 1992 to 1999, he worked as a Head Researcher at National Institute of Animal Industry. He is currently a Professor in the Department of Laboratory Sciences School of Health science, Faculty of Medicine at the University of Kanazawa, Kanazawa, Japan. His research interests include biomedical instrumentation, noninvasive and ambulatory measurement system of health care.



Yumi Kanemitsu graduated from Kansai University, Osaka, Japan, in 1991.

She is with SRI R&D Ltd., developing a noninvasive system which measures heart rate and breathing rhythm during sleep.



Kei-ichiro Kitamura received the B.S. degree in industrial chemistry from Fukui University, Fukui, Japan, in 1978. He received the Ph.D. degree in science from Kanazawa University Graduate School of Natural Science & Technology, Kanazawa, Japan, in 2002.

From 1981 to 1996, he was with the central laboratory of Kanazawa University hospital. He is currently an Associate Professor with the Department of Forefront Medical Technology, Graduate School of Medical Science, Kanazawa University. His current research interests include noninvasive medical measurements of human and bone healthcare sciences using *in vitro* assay systems of scales of goldfish.



Ken-ichi Yamakoshi (M'96) received the D.Med. and D.Eng. degrees from Tokyo Medical and Dental University, Tokyo, Japan, in 1979, and Waseda University, Tokyo, in 1982, respectively.

He was a Research Assistant at Tokyo Women's Medical College from 1972 to 1973, a Research Assistant at Tokyo Medical and Dental University from 1974 to 1980, an Associate Professor at Hokkaido University, Sapporo, Japan, from 1980 to 1994, and has been a Professor at Kanazawa University, Kanazawa, Japan, since 1994. He is also currently a Visiting Professor at Dalian University, Dalian, China, and at Waseda University, Tokyo. His current research interests include noninvasive physiological measurements and instrumentation, health care monitoring, human support systems, cardiovascular biomechanics, and rehabilitation engineering.



Daming Wei (M'92) received the B.Eng. degree from Dept of Mathematics and Mechanics, Tsinghua University, Beijing, China. He received M.Eng. degree from Dept. of Computer Engineering, Shanghai Institute of Technology (Shanghai University), and Ph.D. degree in Biomedical Engineering, Zhejiang University.

He is Professor at faculty of Computer Science and Engineering and director of Information Systems and Technology Center (ISTC), University of Aizu, Japan. Prof. Wei is well known for research and development of state-of-the-art computer heart model and simulation of electrocardiogram. Recent directions in his group include biomedical modeling and computer simulation, visualization and biomedical virtual reality, biomedical informatics, e-health and mobile healthcare. Prof. Wei serves as a council member of International Society of Bioelectromagnetism, and an editor of International Journal of Bioelectromagnetism. He is a council member of Japan Society for Medical and Biological Engineering Tohoku Branch. He is founder and co-chair of IEEE International Conference on Computer and Information Technology. He is leader of several large-scale research projects supported by Central or prefecture government funds focused on academia-industry cooperation. He is founder and CEO of a university venture business company-QRS Corporation. He is also guest professor at several universities in Japan and China.